Invasive behavior of lineage-structured cell populations: The interaction of noise and feedback

June 7, 2012

Shabnam Moobed, Deaprtment of Mathematics, University of California, Irvine, CA
John Lowengrub, Department of Mathematics, University of California, Irvine, CA
Haralampos Hatzikirou, Helmholtz Center for Infectious Disease, Braunschweig, Germany

Abstract

In this paper we develop a stochastic mathematical model, to study the dynamics of growing cell clusters where there is a progenitor-progeny relationship between the cells, regulated by negative feedback. One cell type mimics the combined effects of stem cell and progenitor cells while the other characterizes terminally differentiated cells. We first give a microscopic (stochastic) derivation of the model. Then using averaging and a mean field approximation, we derive a macroscopic (deterministic) description of the model. We focus on investigating the speed and instability of invasive fronts. Our main results indicate that instability develops as a consequence of the interaction between feedback and local stochastic fluctuations. Front instability is not observed in the mean-field model. Our analysis shows that front instability depends on spatial heterogeneity in cell types at the front that arises from strong feedback on the self-renewal probabilities of the stem/progenitor cells from terminally differentiated cells. This is consistent with experimental observations. The front speed is mainly controlled by the self-renewal capacity of the stem cells, the cell motilities, the proliferation and death rates. These are also critical parameters in mean field models. These results have important consequences on the progression of locally invasive tumors and their treatment.

Author Summary

[150-200 words]

1 Introduction

Cancer describes a group of genetic and epigenetic diseases, characterized by uncontrolled growth of cells, and leads to a variety of pathological consequences and frequently death. Cancer has long been recognized as an evolutionary disease [37]; Cancer progression can be depicted as a sequence of traits or phenotypes that cells have to acquire if a neoplasm (benign tumor) is to become an invasive and malignant cancer. A phenotype refers to any kind of observed morphology, function or behavior of a living cell. Hanahan and Weinberg [36] identified six cancer cell phenotypes: unlimited proliferative potential, environmental independence for growth, evasion of apoptosis, angiogenesis, invasion and metastasis. Recently they added two other phenotypes: deregulation of cellular energetics and avoidance of immune destruction [41].

There is now a substantial body of work shows that not all proliferating cells in a tumor matter equally e.g., [16], [17]. There is a small population of cells capable of initiating cancer known as cancer initiating cells or cancer stem cells. These cells were first identified in leukemia [38], [29], [30]. Later, cancer stem cells were formed in solid tumors including breast [15], brain [18], [19], prostate [20], melanoma [21], [22], colon [23], [24], liver [26], [25], and lung [27].

Stem cells are characterized by the ability to self-renew through symmetric and asymmetric cell division and differentiate into a diverse range of specialized cell types. Recent advances in stem cell biology have led to the cancer stem cell hypothesis [28], which states that tumors contain a few cells (cancer initiating cells CIC or cancer stem cells CSC) that are capable of regenerating tumors and many kinds of cells that do not have this capability [19].

Most normal tissues are hierarchically organized into lineages and biologists have come to view cell lineages as fundamental units of tissue and organ development, maintenance, and regeneration. A lineage is a set of progenitor-progeny relationships in which progressive changes in cell character occur. Typically, lineages are traced back to a self-perpetuating stem cell (S), and end with a terminally differentiated cell (T) that is either dying, or has a limited life span. In between stem and terminal cells lie any number of committed progenitor (CP) cell stages. Like S cells, their progeny may remain at the same stage, or move on to a subsequent one (differentiate), however they do not normally self-perpetuate, i.e. they eventually all differentiate.

Lineages provide the framework for "growth control" of tissue and organs. It has long been thought that homeostasis in tissues must be controlled by feedback with signals coming from various the differentiated cells affecting the behavior of the progenitor and stem cells [39], [40]. Recently through the study of feedback growth control by members of the TGFβ superfamily in mammalian epithelium feedback on the self-renewal probability (p) has been shown to be the basis for a powerful control strategy [1], [2]. In general, TGFβ superfamily members have been found to play a role in self-renewal and differentiation of stem cells both in normal tissues and in cancer (e.g., [33], [34], [35]). For example negative feedback regulation of p values as well as division rates υ, explains why a tissue can maintain a fixed size despite fluctuations in cell death rates, stem cell numbers or other parameters. Also negative feedback regulation on p and υ can explain, why fast regeneration occurs after injury [42]. An exciting recent development in cancer biology is the recognition that lineage progression continues to occur in tumors. However the role that lineages play in tumor progression remains unknown.

An important research direction for solid tumors is understanding the role that stem cells and their lineages play in tumor progression. Stem cells are hypothesized to play critical roles in tumorgenesis, tumor progression, resistance to treatment, local invasion and metastasis. Here we focus on modeling the dynamics near a solid tumor front, incorporating lineage relationships and feedback processes among its multicellular components. In particular, important questions we address include: what are the important factors which create an unstable invasive and fast moving front? What role does the spatiotemporal heterogeneity and cell

distribution of cells play in the front dynamics? How do the different cell types affect the front speed and instability, and how important are stochastic fluctuations?

There are many discrete models of solid tumor growth. See the recent reviews [43], [44], [45], [46]. Here we focus on a few that are most relevant to our work. Generally models focus either on continuum or discrete description of cells and their behavior, although there are new hybrid methods that combine these descriptions, [47]. Enderling et. al. [10], [12], [11] developed a cellular automata-based computational model which tracks the fate of individual cancer cells, applying basic rules for cell proliferation, differentiation, migration and cell death. In this model a lineage with two motile constituents (e.g. stem cells and terminally differentiated cells) are simulated. The only feedback between the different cell types is through the spatial limitations of growth (e.g. only one cell can occupy a node on the computational grid). Enderling et. al. conclude counterintuitively that, when the proliferation capacity of non-stem cells is relatively low, and the rate of cell death is high, tumor growth is accelerated. This is because when cells die faster there will be more space available for stem cells to proliferate.

Sottoriva et. al. [9], [8] developed a tumor growth model based on cellular automata and partial differential equations, which simulates proliferation, differentiation, metabolism and migration. The model investigates the consequences of a hierarchically organized cancer cell population (cancer stem cells and non stem cells) on the dynamics of solid tumor growth. They conclude cancer hierarchal organization promotes phenotypical heterogeneity, and small number of lightly motile CSCs promote the development of invasive tumor morphologies and micro-satellite fractions. Enderling et. al. and Sottoriva et. al. did not explicitly include feedback, only spatial limitation, which is a type of contact-inhibition feedback on proliferation. In related work Hatzikirou et.al. [7] developed a Lattice Gas Cellular Automata model and investigated the go-or-grow mechanism by which a transition from a benign neoplasm tumor (highly proliferative) to a malignant invasive tumor (high migration) may occur as a consequence of transitions between these two phenotypes.

Very recently Youssefipour et. al. [48] has developed a multispecies continuum model to simulate the dynamics of cell lineages in solid tumors. The model considers spatiotemporally varying cell proliferation, differentiation and death mediated by the heterogenous distribution of oxygen and soluble substrates (e.g. feedback factors that affect the self-renewal and division rates). Together these regulate the rate of self-renewal and division of the different cells within the lineages. Terminally differentiated cells release negative feedback factors (e.g., from the TGFβ superfamily of proteins) that decrease rates of self-renewal and proliferation rates of less differentiated cells. Stem cells release a short-range positive feedback factor (e.g., Wnt), as well as a long-range inhibitor (e.g., Dkk). Results show that the strength of the feedback from the TGFβ family influence the morphology and total volume of the tumor. A low level of feedback makes the tumor grow rapidly and become invasive. Also the interaction among the factors plays an important role in the formation of spatial patterns (e.g. stem cell niches) and the heterogeneous distribution of the lineage components.

In this paper, we extend the LGCA model to simulate the spatiotemporal dynamics of cell lineages in normal tissues and in tumors. Cells are represented as discrete, stochastic entities that may proliferate, differentiate and may move throughout a grid in space. The differentiated cells negatively feedback on the self-renewal probabilities of stem cells, increasing their probability to differentiate. This model is limited to small (e.g., cell) scale processes. We then investigated the speed and stability of an advancing tumor as a function of the feedback processes and the conditions in the tumor microenvironment.

2 Results and Discussion

2.1 Spatially heterogeneous systems

In this paper, we consider the evolution arising from spatially non-uniform initial data. In particular, we consider the evolution of a propagating front. As initial data, we take a rectangular strip of S cells located in randomly selected channels in the first four grid points on the left hand side (LHS) of the domain. No-flux boundary conditions are imposed at the LHS of the domain, periodic boundary conditions are used at the top and bottom of the domain, and cells that more beyond the right hand side of the domain are removed from the system (open boundary conditions). Next we determine the sensitivity of these results to parameter variations.

1) change of node capacity N: We now investigate the effect of node capacity N. In Fig. 3a front instability and front position at a fixed time step ($T = 15000$) are shown as a function node capacity. The maximum node capacity ranges from N=4 to N=24, while the other parameters $\bar{p} = 0.7, \alpha = 3, D_S = 1/4, D_T = 1/4, d = .05$ are fixed. Each data point on a figure is an average over 30 simulations and standard deviation (STD) bar is shown. For front position the STD is negligible. By increasing node capacity N, number of rest channels at each node increases which results in a slower moving front as Fig. 3a confirms. Moreover increasing node capacity decreases the on-node fluctuations in LGCA which predicts no front instability. Note that in mean field approximation, N is assumed large. Consistent with this, the MF-PDE predicts front propagation is stable. Taken together these results imply that front instability is a noise induced phenomena. In particular, the instability does not depend on non linearity, but on rather the on-node fluctuations.

2) change of feedback strength α: In Fig. 3b, we analyze the effect of feedback on front invasion. In this figure the left axis shows the magnitude of the dominant Fourier mode and the right axis shows the front position for different feedback strengths $\alpha = 1, 2$ and 3 at a fixed time step $T = 15000$. The numbers in the box is r, where Increasing α, increases front instability. Although increasing α decreases front speed. A snapshot of a simulation at $T = 15000$ is shown for two extreme node capacity cases $\alpha = 1$, $\alpha = 2$ and $\alpha = 3$. Each data point in the figure is average over 30 simulations and standard deviation bar is shown for each data points. For front position the std is negligible.

3) change in S and T cell motility:
I) effect of different motilities on instability mechanism: D_S and D_T can be modified by introducing different numbers of rest channels in the S and T lattices. Depending on SC and TDC motilities there are two mechanisms for front instability. Fig. 4a,b) shows the evolution of spatiotemporal pattern formation in the LGCA model over three time steps, T = 15000, T = 15050, T = 15100. A zoom in the front region in the rectangular box are shown. S and T populations are shown where the blue color marks regions with large T densities and red marks regions with large S densities. If S cells and T cells have the same motility, as the front propagates, S cells detach and move ahead of the front. These S cells thus escape feedback regulation and begin to proliferate and differentiate, forming micro clusters that become subsumed by the propagating front, which results in propagating fingers as shown in Fig. 4a). Similar instability mechanism was identified by Enderling et. al. [10] as self-metastasis and by Sottoriva et.al. [9] in the context of growing circular cell clusters, where feedback was associated with spatial limitations on cell division rates. The detachment process, micro-satellite growth and absorption into the front is illustrated in Fig. 4a), where circles denote proliferation events. If T cells are more motile than S cells, the S cell fraction at the front decreases compared to the case with equal motilities, therefore the SCs are less able to escape from the bulk. However, the death of TD cells creates empty spaces and opportunities for SCs to proliferate and differentiate. This can lead to the development of propagating fingers over time which is shown in Fig. 4b).

II) effect of different motilities on front speed: In Fig. 5a) front position is shown as a function of different ratio of cell motilities (D_S/D_T) at a fixed time T=15000. Each data point is an average over 30

simulations. Front position is defined to be the overall mean of the cell positions in the front region. S cell fraction is shown in different regions of the 9 quantiles of the front and the bulk in Fig 5b). As these results show as the ratio of S over T cell motility decreases there is less S cell fraction in the more advanced front quantiles as well as lower S cell fraction in bulk which creates a slower front. This pattern does not follow for the case $D_S/D_T = 1$ since as we see in this case the tip S cell density (regions 1, 2, 3) is at 0.11, where for 5 is 0.18 and 4 is 0.14.

III) effect of different motilities on front instability: In Fig. 6a) magnitude of the Fourier dominant mode is shown as a function of different ratio of cell motilities (D_S/D_T) at a fixed time $T = 15000$. Each data point is an average over 30 simulations and bars show standard deviation at each point. In Fig 6b) Detachment of S cell fraction is shown in different regions of the 9 quantiles of the front and the bulk. As the ratio S over T cell motility decreases results in more S cell detachment specifically in the lower front regions. This creates larger instability. When $D_S/D_T = 1$, we see a pick in the instability diagram which can be explained by looking at the regions of S cell detachment in the front. In this case we see larger detachment of S cell from all the quantiles of the front which is different from other motility ratio cases. We quantify the detachment of S cells by calculating maximum distance of a S cell from other cells over all rows at the time step.

3 Methods and Models

(Note: This section should be modified and reduced to a couple of pages only)

3.1 Introduction to LGCA

An advantage of the LGCA method is that collisions of particles at lattice sites are avoided. Implementing movement of individuals in traditional cellular automaton models is not straightforward, as one site in a lattice can typically only contain one individual. Consequently movement of individuals causes collisions when two individuals move to the same empty site, and this needs to be resolved (e.g., see [3] for a discussion). In the LGCA model this problem is avoided by having separate channels for each direction of movement and imposing an exclusion principle on channel occupation, namely that each channel may host at most one particle. The channels specify the direction and magnitude of movement, which may include zero velocity (resting) states. For example, a square lattice has four non-zero velocity channels and an arbitrary number of rest channels.

The LGCA was first introduced to model a flow of a gas as a fully discrete system, the so-called Hardy, de Pazzis, and Pomeau (HPP) model [5]. The HPP model used a square lattice, where the gas particle motion in the coordinate directions was defined by momentum conserving collisions of gas particles. LGCA model since been used to simulate the behavior of a particle flow in large scale [4] .

The dynamics of a LGCA arises from repetitive application of superpositions of local (probabilistic) interaction and deterministic propagation (transport) steps applied simultaneously to all lattice nodes at each discrete time step. The definitions of these steps have to satisfy the exclusion principle, i.e. two or more particles are not allowed to occupy the same channel at a single node. The interaction rule regulates the particle motion redistribution, and the birth/death of particles. In the propagation step, individuals move synchronously into the direction and by the distance specified by their velocity state. The propagation step is deterministic and conserves mass and momentum. Synchronous transport prevents individual collisions that would violate the exclusion principle (other approaches have to define a collision resolution algorithm). Therefore, LGCA models allow parallel synchronous movement and fast updating of a large number of individuals [7].

3.2 LGCA States and definitions

We consider a LGCA defined on a two-dimensional regular lattice $\mathcal{L} = L_1 \times L_2 \subset \mathbb{Z}^2$, where L_1, L_2 are the lattice dimensions. Cells move on the lattice with discrete velocities, i.e., they hop at discrete time steps from a given node to a neighboring one, as determined by the speed associated with the channel in which they reside [6]. The set of velocities for the square lattice, which is considered here, is represented by the two-dimensional channel velocity vectors: $\boldsymbol{c}_1 = \begin{pmatrix} 1 \\ 0 \end{pmatrix}, \boldsymbol{c}_2 = \begin{pmatrix} 0 \\ 1 \end{pmatrix}, \boldsymbol{c}_3 = \begin{pmatrix} -1 \\ 0 \end{pmatrix}, \boldsymbol{c}_4 = \begin{pmatrix} 0 \\ -1 \end{pmatrix}$. In each of these channels, we consider an exclusion principle and allow at most one cell per channel. We denote by $\tilde{b} = b + \beta$ the total number of channels per node which can be occupied simultaneously, where β is the number of channels with zero velocity, the so-called rest channels. The parameter b is the coordination number, i.e. the number of velocity channels on a node. In particular, $b = 4$ for the square lattice. We represent the channel occupancy by a Boolean random variable $\eta_i(\boldsymbol{r}, k) \in \{0, 1\}$, where $i = 1, \ldots, \tilde{b}, \boldsymbol{r} = (r_x, r_y) \in \mathcal{L} \subset \mathbb{Z}^2$ is the spatial variable denotes the lattice node and $k \in \mathbb{N}$ is the time variable. The $\tilde{b}$-dimensional vector

$$\boldsymbol{\eta}(\boldsymbol{r}, k) = (\eta_1(\boldsymbol{r}, k), \ldots, \eta_{\tilde{b}}(\boldsymbol{r}, k)) \in \mathcal{E},$$

is called the node configuration and $\mathcal{E} = \{0, 1\}^{\tilde{b}}$ is the automaton state space. The node density is the total number of cells present at a node $r \in L$, and denoted by:

$$n(r, k) := \sum_{i=1}^{\tilde{b}} \eta_i(\boldsymbol{r}, k)$$

3.3 LGCA for cell lineages

In this section, we develop a LGCA for lineages containing cells with two states of differentiation. We represent non occupied tissue by empty channels and we model explicitly two cell "species", denoted by $\sigma \in \sum = \{S, T\}$: Stem cells (S) and terminally differentiated cells (T), analogously. We allow the movement of these populations in two different parallel lattices $\mathcal{L}_\sigma = \{\mathcal{L}_S, \mathcal{L}_T\}$ as depicted in figure 1. We assume each node in lattice S consists of $\tilde{b}_S$ channels and respectively each node in lattice T consists of $\tilde{b}_T$ channels. We allow at most $N = \min\{\tilde{b}_S, \tilde{b}_T\}$ cells at each node. We can relate N to the microenvironmental conditions (e.g., nutrient). We can assume nutrient is proportional to free space i.e. small N implies low supply of nutrients, which can mimic the effect of unfavorable microenvironment . Accordingly, we define $n_\sigma(r, k)$ and $\eta_\sigma(r, k)$ to be the node density and configuration respectively of lattice σ.

The automaton dynamics arises from the Propagation (P) of cells from one node to a neighboring node, the reorientation (O) of cells from one channel to another (e.g., reshuffling) and cell kinetics (R), which changes the number of cells at a node (e.g. birth/death, differentiation). Thus, the node configuration is updated in time by

$$\eta_{\sigma,i}(\boldsymbol{r} + \boldsymbol{c}_i, k + 1) = POR(\eta_{\sigma,i}(\boldsymbol{r}, k))$$

at each time step where every node in the lattice is updated independently of every other node.

3.3.1 Propagation (P)

The propagation step is deterministic and is defined by an operator P. The application of P transports all the cells simultaneously to the neighboring nodes in the direction of their velocity.

3.3.2 Reorientation (O)

The reorientation operator is responsible for the stochastic redistribution of cells within the velocity channels of a given node, providing a new node velocity distribution. We assume that cells are randomly distributed

according to a uniform distribution among the channels at each node. The corresponding transition probabilities are

$$P(\eta_\sigma \to \eta_\sigma^O)(\mathbf{r},k) = \frac{1}{Z}\delta(n_\sigma(\boldsymbol{r},k), n_\sigma^O(r,k)), \tag{1}$$

where η_σ^O corresponds to the node configuration after reorientation and $n_\sigma^O(r,k)$ is the corresponding density. The normalization factor $Z = \binom{\tilde{b}}{n_\sigma(\boldsymbol{r},k)}$ corresponds to the number of different ways of placing $n_\sigma(r,k)$ cells into the $\tilde{b}_\sigma$ channels. The Kronecker δ, when $\delta(x,y) = 0$ unless $x = y$ and $\delta(x,x) = 1$, guarantees the mass conservation of this operator.

3.3.3 Cell Kinetics (R)

On the S lattice two reaction processes are taken into account: self-renewal and differentiation. Self-renewal refers to the fact that S cells may replenish their numbers. We assume that a S cell can divide into 2 S cells upon division with with a probability p and a mitosis rate of υ only if there is enough space on the S lattice. For simplicity we do not distinguish between symmetric and asymmetric division since this does not change S numbers. We assume that stem cells can differentiate upon division with probability $1-p$ only if they there are at least two empty channels in the corresponding node in the T lattice.T cells do not renew their numbers and die at a rate d. At each time step the reaction step is performed for each node on both the S and T lattices. Only one reaction step is performed per node and occurs at a randomly selected channel. The offspring is also put In a randomly selected channel at that node or, in the case of differentiation of a S cell, at the corresponding node on the T lattice.

We add negative feedback as depicted in Fig. 2 to the model by requiring that the self-renewal probability p at each node be a function of the T cell density at the corresponding node. In particular we take p to be

$$p = \bar{p}(1 - \frac{n_T(r,k)}{N})^\alpha$$

where α is a strength feedback parameter and $\bar{p}$ is the self-renewal probability if there are no T cells. More realistically, the feedback should depend on contact of S cells with their neighbors as well soluble feedback factors. At each time step there are three events that can occur to change the node density at both lattices. These three events are, (i) a new channel may be occupied at node r of lattice S (self-renewal) (S_1), (ii) 2 new channels may be occupied at node r of lattice T (differentiation) (S_2), and a (iii) channel in lattice T becomes unoccupied (death of T cell) (T_d).
The probability of each event is:

$$P(S_1) = \frac{1}{N}\upsilon\frac{n_S}{N}\frac{N-n_S}{N}\bar{p}(1-\frac{n_T}{N})^\alpha,$$

$$P(S_2) = \frac{1}{N}\upsilon\frac{n_S}{N}\frac{N-n_T}{N}\frac{N-n_T-1}{N-1}(1-\bar{p}(1-\frac{n_T}{N})^\alpha),$$

$$P(T_d) = \frac{1}{N}\frac{n_T}{N}d,$$

where $n_S(r,k)$ and $n_T(r,k)$ are the total number of cells at node r at time k in lattices S and T respectively. Furthermore in order for S cells to self-renew or differentiate there should be enough space in the correspondent lattice. The terms $\frac{N-n_S}{N}$ and $\frac{N-n_T}{N}\frac{N-n_T-1}{N-1}$ represent these assumptions. Consequently the self-renewal and differentiation probabilities also depend on the number of S cells and T cells, which corresponds to feedback from spatial restrictions.

3.4 Mean Field Approximation

An advantage of the LGCA modeling framework is that there are well developed upscaling methodologies to obtain equations govern the average behavior of the system. Accordingly in this section we upscale the lineage LGCA and obtain the mean-field (MF) equations that describe the dynamics of the average cell densities.

3.4.1 Mean field dynamics for cell kinetics

We first derive the mean field dynamics for the reaction kinetics R. Essentially, this corresponds to a well-stirred assumption where the node location r parameterizes the evolution. Following (REF), we use a transition matrix approach since the evolution process $\{(n_S, n_T)_k\}_{k\in\mathbb{N}}$ is a Markov chain with state space $S = \{(n_S, n_T)|n_S, n_T \in \{0, \dots N\}\}$. Note that there are $|S| = N^2$ possible states of the system.

Let $P_{n_\sigma}(r, k)$ be the probability of finding n cells on lattice $\sigma = S, T$. Then,

$$P_{n_\sigma}(r, k+1) - P_{n_\sigma}(r, k) = \sum_{n_{\sigma'}} \hat{W}^R_\sigma(n_\sigma, n_{\sigma'}) P_{n_{\sigma'}}(r, k) \tag{2}$$

where $W^R_\sigma(n_\sigma, n_{\sigma'})$ is the transition probability matrix that describes the probability of a transition from $n_{\sigma'}$ to n_σ by the cell kinetics operation. That is, $\hat{W}^R_\sigma(n_\sigma, n_{\sigma'}) = P(n_\sigma|n_{\sigma'})$, where $P(n_\sigma|n_{\sigma'})$ is the conditional probability of the next state n_σ given the current state $n_{\sigma'}$. This can be calculated as follows. From Bay's rule [49], we may write

$$P(n_S|n_{S'}) = \frac{1}{P(n_{S'})} \sum_{n_T} \sum_{n_{T'}} P(n_S, n_T|n_{S'}, n_{T'}) P(n_S, n_T) \tag{3}$$

where $P(n_{S'})$ is the probability of achieving state $n_{S'}$, $P(n_S, n_T|n_{S'}, n_{T'})$ is the conditional probability of the state (n_S, n_T) given the state $(n_{S'}, n_{T'})$, and $P(n_{S'}, n_{T'})$ is the probability of state $(n_{S'}, n_{T'})$.The transition matrix of the process is defined as

$$\hat{W}^R_\sigma(n_S, n_T; n_{S'}, n_{T'}) = P(n_{S'}, n_{T'}|n_S, n_T)$$

which is calculated in the Appendix. An analogous formula holds for $P(n_T|n_{T'})$.

To make further progress we assume that :

$$P(n_S, n_T) = P(n_S)P(n_T)$$

That is the cell kinetics in the S and T lattices are independent. Of course, this is a rather coarse approximation because differentiation of S cells produces T cells, and T cells regulate the feedback on the self-renewal probability of the S cells. Putting everything together, we obtain :

$$\hat{W}^R_S(n_S, n_{S'}) = \sum_{n_T} P(n_T) \sum_{n_{T'}} W(n_S, n_T, n_{S'}, n_{T'}) \tag{4}$$

$$\hat{W}^R_T(n_T, n_{T'}) = \sum_{n_S} P(n_S) \sum_{n_{S'}} W(n_S, n_T, n_{S'}, n_{T'}) \tag{5}$$

In the Appendix, it is shown that W_S^R and W_T^R can be written as:

$$\begin{aligned}\hat{W}_S^R(n_S, n_S') = &\frac{\upsilon\bar{p}(\frac{N-\rho_T}{N})^\alpha}{N^2}(\frac{n_S(N-n_S)}{N})\delta_{n_S-1,n_S'} \\ &+ \upsilon\frac{n_S(1-\bar{p}(\frac{N-\rho_T}{N})^\alpha)}{N^3(N-1)}(N-n_T)(N-n_T-1)\delta_{n_S+1,n_S'} \\ &- \frac{\upsilon\bar{p}(\frac{N-\rho_T}{N})^\alpha}{N^2}(\frac{n_S(N-n_S)}{N})\delta_{n_S,n_S'} \\ &- \upsilon\frac{n_S(1-\bar{p}(\frac{N-\rho_T}{N})^\alpha)}{N^3(N-1)}(N-\rho_T)(N-\rho_T-1)\delta_{n_S,n_S'},\end{aligned}$$

and

$$\begin{aligned}\hat{W}_T^R(n_T, n_T\prime) = &\frac{n_T d}{N^2}(1-\upsilon\frac{\rho_S(1-\bar{p}(\frac{N-n_T}{N})^\alpha))}{N^3(N-1)})(N-n_T)(N-n_T-1))\delta_{n_T+1,n_T\prime} \\ &+ \frac{n_T d}{N^2}\upsilon\frac{\rho_S(1-\bar{p}(\frac{N-n_T}{N})^\alpha)}{N^3(N-1)}(N-n_T)(N-n_T-1))\delta_{n_T-1,n_T\prime} \\ &+ (1-\frac{n_T d}{N^2})\upsilon\frac{\rho_S(1-\bar{p}(\frac{N-n_T}{N})^\alpha)}{N^3(N-1)}(N-n_T)(N-n_T-1))\delta_{n_T-2,n_T\prime} \\ &- (1-\frac{n_T d}{N^2})(1-\upsilon\frac{\rho_S(1-\bar{p}(\frac{N-n_T}{N})^\alpha)}{N^3(N-1)})(N-n_T)(N-n_T-1))\delta_{n_T,n_T\prime}\end{aligned}$$

where $\rho_S(\mathbf{r},k) = \sum_{n_{S'}} n_{S'} P_{n_{S'}}(\mathbf{r},k)$ and $\rho_T(\mathbf{r},k) = \sum_{n_{T'}} n_{T'} P_{n_{T'}}(\mathbf{r},k)$

Now, to obtain an equation for ρ_σ, we multiply equation (2) by n_σ and sum over n_σ. Further, assuming independency of the channels e.g. ignoring all on node correlations, we obtain the system :

$$\rho_S(r,k+1)-\rho_S(r,k) = \frac{1}{N}\frac{\rho_S}{N}\upsilon\bar{p}(\frac{N-\rho_T}{N})^\alpha\frac{(N-\rho_S)}{N} - \frac{1}{N}\frac{\rho_S}{N}\upsilon(1-(\bar{p}\frac{N-\rho_T}{N})^\alpha)\frac{(N-\rho_T)(N-\rho_T-1)}{N(N-1)}, \quad (6)$$

$$\rho_T(r,k+1) - \rho_T(r,k) = 2\frac{1}{N}\frac{\rho_S}{N}\upsilon(1-\bar{p}(\frac{N-\rho_T}{N})^\alpha)\frac{(N-\rho_T)(N-\rho_T-1)}{N(N-1)} - \frac{1}{N}\frac{\rho_T d}{N} \quad (7)$$

which are the mean field growth laws for the average cell densities.

To describe the behavior at the macro-scale, we use a parabolic scaling and scale time as $t = \epsilon^2 k$ and $x = \epsilon r$. We then obtain $\rho_\sigma(r,k+1)-\rho_\sigma(r,k) = \epsilon^2\partial_t\tilde{\rho}_\sigma(x,t)+O(\epsilon^3)$, where $\tilde{\rho}_\sigma(x,t) = \rho_\sigma(\frac{r}{\epsilon},\frac{k}{\epsilon^2})$. Accordingly, the macroscopic mitosis and death rates are obtained as $\tilde{\upsilon} = \frac{\upsilon}{\epsilon^2}$ and $\tilde{d} = \frac{d}{\epsilon^2}$ respectively. Taking the limit $\epsilon \to 0$, assuming $\tilde{\upsilon}$ and $\tilde{d}$ remain bounded, we obtain the macroscopic system (dropping the tilde notation)

$$\partial_t\rho_S(x,t) = F_S(\rho_S,\rho_T), \quad (8)$$

$$\partial_t\rho_T(x,t) = F_T(\rho_S,\rho_T), \quad (9)$$

where

$$F_S(\rho_S,\rho_T) = \frac{1}{N}\tilde{\upsilon}\frac{\rho_S}{N}\bar{p}(\frac{N-\rho_T}{N})^\alpha\frac{(N-\rho_S)}{N} - \frac{1}{N}\tilde{\upsilon}\frac{\rho_S}{N}(1-\bar{p}(\frac{N-\rho_T}{N})^\alpha)\frac{(N-\rho_T)(N-\rho_T-1)}{N(N-1)}, \quad (10)$$

$$F_T(\rho_S,\rho_T) = 2\frac{1}{N}\tilde{\upsilon}\frac{\rho_S}{N}(1-\bar{p}(\frac{N-\rho_T}{N})^\alpha)\frac{(N-\rho_T)(N-\rho_T-1)}{N(N-1)}, -\frac{1}{N}\frac{\rho_T\tilde{d}}{N} \quad (11)$$

are the macroscopic reaction terms. Note that in Eqs. (8) - (9), the spatial coordinate x is a parameter. We next consider the effect of spatial variations and we account for the reorientation and propagation operations.

3.4.2 MFA of spatiotemporal dynamics

In the previous section, we derived the mean-field approximation under a spatially homogeneous system (well-stirred system) assumption. Here, we demonstrate how to derive a spatiotemporal mean-field approximation of the growth LGCA model for a spatially distributed system. The spatiotemporal dynamics is fully specified by the following microdynamical equations:

$$\eta_{i\sigma}(\boldsymbol{r}+\boldsymbol{c}_i,k+1)=\sum_{j=1}^{\tilde{b}}\mu_j(\boldsymbol{r},k)\eta^R_{j\sigma}(\boldsymbol{r},k), \tag{12}$$

$$\eta^R_{i\sigma}(\boldsymbol{r},k)=\eta_{i\sigma}(\boldsymbol{r},k)+R_{i\sigma}(\boldsymbol{r},k), \tag{13}$$

where the $R_{i\sigma}$ models the reaction kinetics of a cell on a node $\mathbf{r}$ at time k. Assuming that the mean field reaction is independent of cell direction, so that birth is independent of orientation, we can define $R_{i\sigma}=F_\sigma/\tilde{b}=\bar{R}_\sigma$ where F_σ are giving by (10) and (11), which is the mean field growth law for a single node. Eq. (12) describes the redistribution of cells on the velocity channels and the propagation to the neighboring nodes. Eq. (13) defines the new occupation number after the application of the growth operator R. We introduce the average change of the occupation number of channel i, where $i=1,\ldots,b$, $f_i=\langle\eta_i\rangle$:

$$f_{i\sigma}(\boldsymbol{r}+\boldsymbol{c}_i,k+1)-f_{i,\sigma}(r,k)=\langle\eta_{i\sigma}(\boldsymbol{r}+\boldsymbol{c}_i,k+1)-\eta_{i\sigma}(\boldsymbol{r},k)\rangle \tag{14}$$

and under the mean-field approximation (MF), where all spatial correlations are neglected, the distribution functions factorize. Combining equations (12), (13) and (14), we obtain

$$f_{i\sigma}(\boldsymbol{r}+\boldsymbol{c}_i,k+1)-f_{i\sigma}(\boldsymbol{r},k)=\sum_{j=1}^{\tilde{b}}\Omega_{ij}f_{j\sigma}(\boldsymbol{r},k)+\sum_{j=1}^{\tilde{b}}(\delta_{ij}+\Omega_{ij})\bar{R}_\sigma(\boldsymbol{r},k), \tag{15}$$

where the matrix $\Omega_{ij}=\frac{1}{\tilde{b}}-\delta_{ij}$ is the transition matrix of the underlying shuffling process (reorientation operator)

3.4.3 Chapman-Enskog method

In order to derive the macroscopic dynamics, we use the Chapman-Enskog methodology [50]. As in section 2.4.1we assume the parabolic (or diffusive) spatio-temporal scaling

$$x=\epsilon r \text{ and } t=\epsilon^2 k \tag{16}$$

where (x,t) are the continuous variables as $\epsilon\to 0$. Using the spatio-temporal scaling relation Eq. (16) and replacing the left hand side of eq. (15) by its Taylor expansion, we obtain

$$f_{i\sigma}(\boldsymbol{r}+\boldsymbol{c}_i,k+1)-f_{i,\sigma}(\boldsymbol{r},k)=(\epsilon^2\partial t+\epsilon^4/2\partial_{tt}+\epsilon\boldsymbol{c}_i\Delta+\epsilon^2/2(\boldsymbol{c}_i.\Delta)^2+\epsilon^2\partial_t(\boldsymbol{c}_i.\Delta))f_{i\sigma}(\boldsymbol{r},k) \tag{17}$$

where $\Delta f=\partial_{xx}+\partial_{yy}$ Further, we assume an asymptotic solution of the single particle distribution f_i in terms of the parameter ϵ:

$$f_{i\sigma}=f^{(0)}_{i\sigma}+\epsilon f^{(1)}_{i\sigma}+\epsilon^2 f^{(2)}_{i\sigma}+O(\epsilon^3) \tag{18}$$

and we assume that the division or death of cells occur on at a much slower time scale than the motion. The idea is that growth can be considered as a perturbation of cell motion. That means that the dominant process is cell diffusion, as shown below. Accordingly, the reaction rate is assumed to be scaled according to the macroscopic time scaling :

$$R_{i\sigma}\to\epsilon^2\tilde{R}_{i\sigma} \tag{19}$$

It follows that the macroscopic birth and death rates scale as $\upsilon=\epsilon^2\tilde{\upsilon}$ and $d=\epsilon^2\tilde{d}$ where $\tilde{\upsilon},\tilde{d}=O(1)$. Therefore, our approach is valid only for very low growth rates.

The macroscopic quantity of interest is the cell density $\rho = \sum_i f_{i\sigma}^{(0)}$, with the assumption $\sum_i f_{i\sigma}^{(l)} = 0$ if $l \geq 1$. This means that only the equilibrium solution $f_{i\sigma}^{(0)}$ contributes to the mass of the system. Plugging Eqs. (16) and (17) into Eq. (15), and matching the powers of ϵ yields:

$$O(1) \quad : \quad \sum_j \Omega_{ij} f_{j\sigma}^{(0)} = 0, \tag{20}$$

$$O(\epsilon^1) \quad : \quad (c_i.\Delta) f_{j\sigma}^{(0)} = \sum_j \Omega_{ij} f_{j\sigma}^{(1)}, \tag{21}$$

$$O(\epsilon^2) \quad : \quad \partial t f_i^{(0)} + (c_i \Delta) f_{i\sigma}^{(1)} + 1/2 (c_i.\Delta)^2 f_{i\sigma}^{(0)} = \sum_j \Omega_{ij} f_{j\sigma}^{(2)} + \tilde{R}_{i\sigma} \tag{22}$$

The solutions of equations (19), (20), (21) are based on the properties of the transition matrix Ω [50] yields the following reaction diffusion equation:

$$\partial_t \rho_\sigma = 1/\tilde{b} \Delta^2 \rho_\sigma + F_\sigma \tag{23}$$

where $F_\sigma = \tilde{b} \bar{R}_\sigma$ is the macroscopic reaction law, i.e. F_S and F_T are as eq. (11) and (12) respectively.

3.5 Acknowledgments

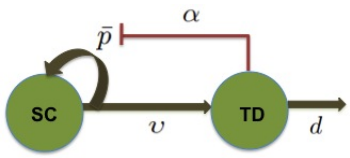

Figure 1: A schematic of a two stage lineage with negative feedback from terminally differentiated cells to self-renewal probability $\bar{p}$ of stem cells. Parameters α, υ and d represent the feedback strength,mitosis rate, and death rate respectively.

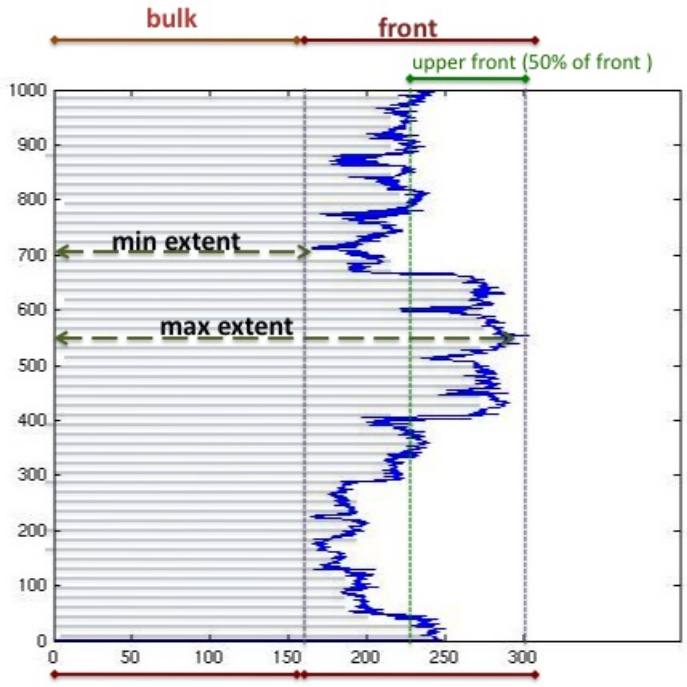

Figure 2: A schematic of a propagating cell front, distinguishing the bulk and the front region (which is subdivided into lower and upper front). We calculate the distance (extent) from the furthest most occupied node to the origin of each row. Front is the region (columns) between the maximum and minimum extent, and bulk is defined to be the region (columns) between minimum extent and origin.

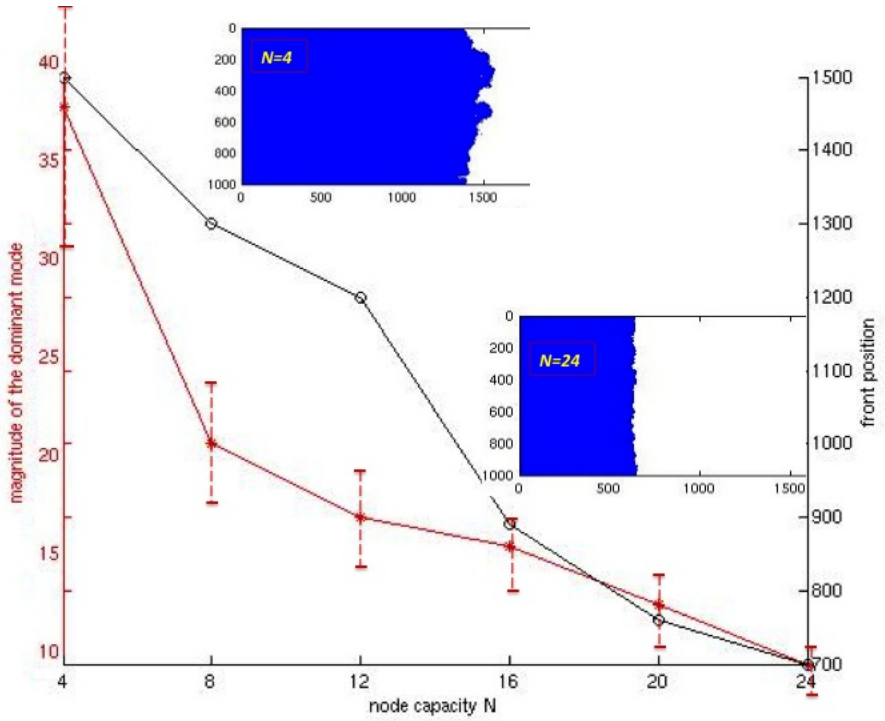

(a) Node capacity & Front invasion

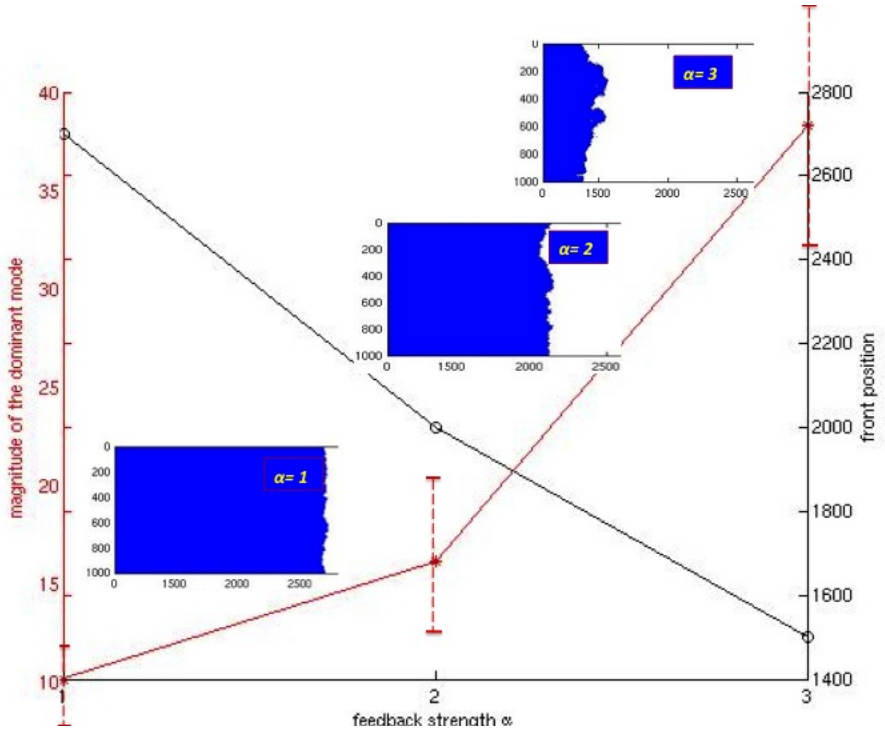

(b) Negative feedback & Front invasion

Figure 3: a) **The effect of node capacity on front invasion (Noise; see explanations in the text):** In this figure front instability and front position at a fixed time step (T=15000) are shown as a function node capacity which changes in the range of 4 to 24. Each data point on a figure is an average over 30 simulations and standard deviation (STD) bar is shown. For front position the STD is negligible. Increasing node capacity, decreases front speed. Moreover increasing node capacity decreases the on-node fluctuations in LGCA which predicts no front instability. A snapshot of a simulation at T=15000 is shown for two extreme node capacity cases $N = 4$ and $N = 24$. b) **The effect of feedback strength on front invasion:** In this figure front instability and front position at a fixed time step (T=15000) are shown as a function feedback strength which changes in the range of 1 to 3. Increasing α, increases front instability. Although increasing α decreases front speed. A snapshot of a simulation at T=15000 is shown for two extreme node capacity cases $\alpha = 1$, $\alpha = 2$ and $\alpha = 3$. Each data point in the figure is average over 30 simulations and standard deviation bar is shown for each data points. For front position the std is negligible. Parameters used in this figure are $\alpha = 3, \bar{p} = 0.7$ and $d = 0.05, D_S = D_T$.

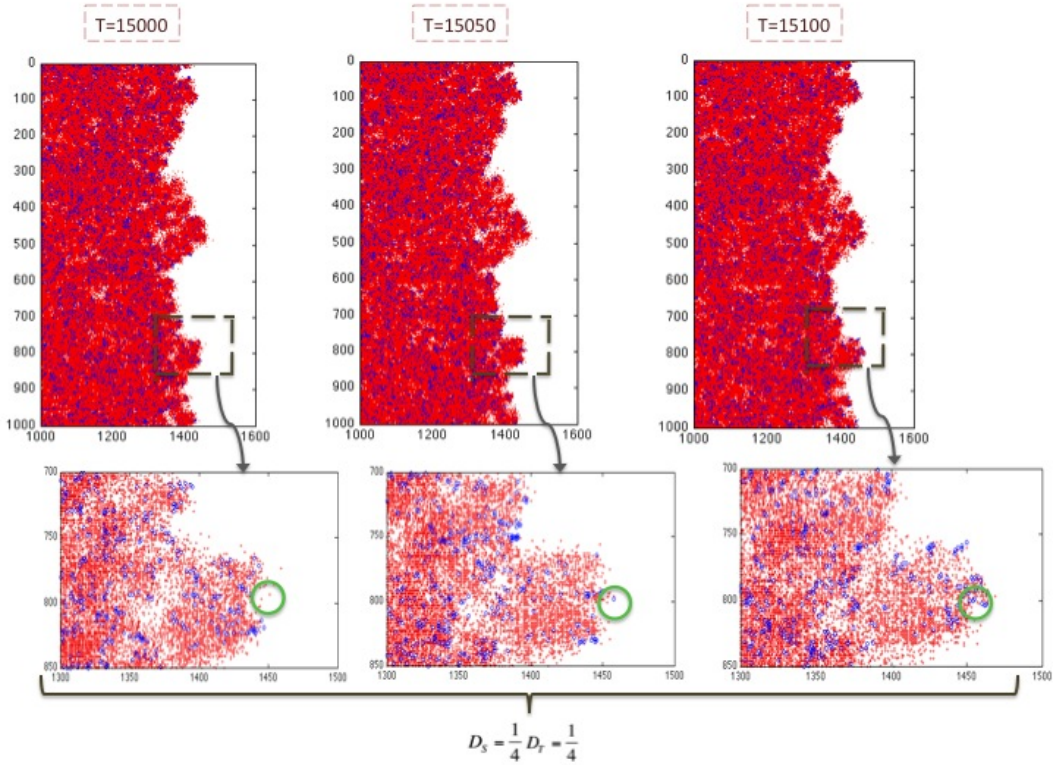

(a) Front instability mechanism I

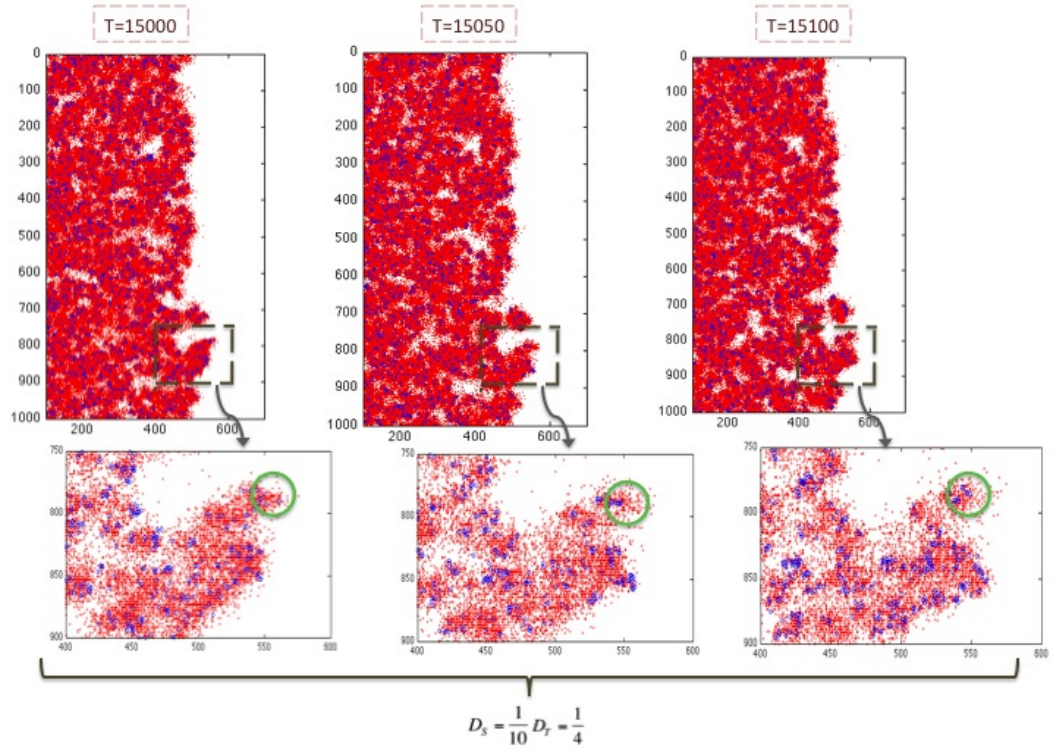

(b) Front instability mechanism II

Figure 4: **Evolution of spatiotemporal pattern formation** in the LGCA model over three time steps ($T = 15000, T = 15050, T = 15100$) as well as zoom in the front region in the rectangular box are shown. Red: high T density, Blue: high stem cell density. 1000×2500 grid is used with no-flux boundary conditions at $x = 0$, open boundary conditions at $x = 2500$ and periodic boundary conditions in the $y-$ direction. The initial condition consists of a strip of S cells populating the first 4 grid points at the left edge of the domain. a) $D_S = D_T = 1/4$: The mechanism for front instability in this case is the detachment process, micro-satellite growth and absorption into the front instability over time. b) $D_S = 1/10, D_T = 1/4$: Death of T cells, creates some space empty, S cells push the front T cells from behind and continue developing the same finger over time.

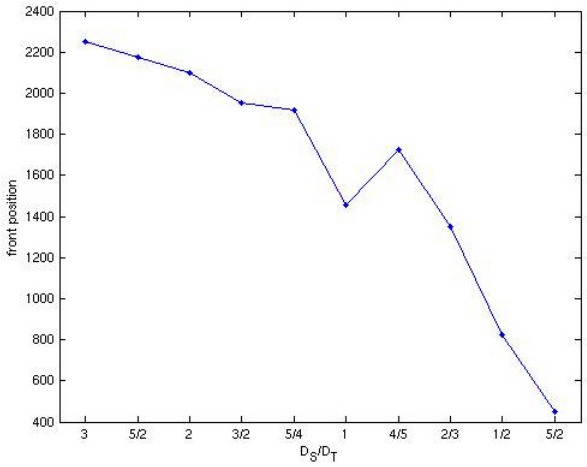

(a) front position

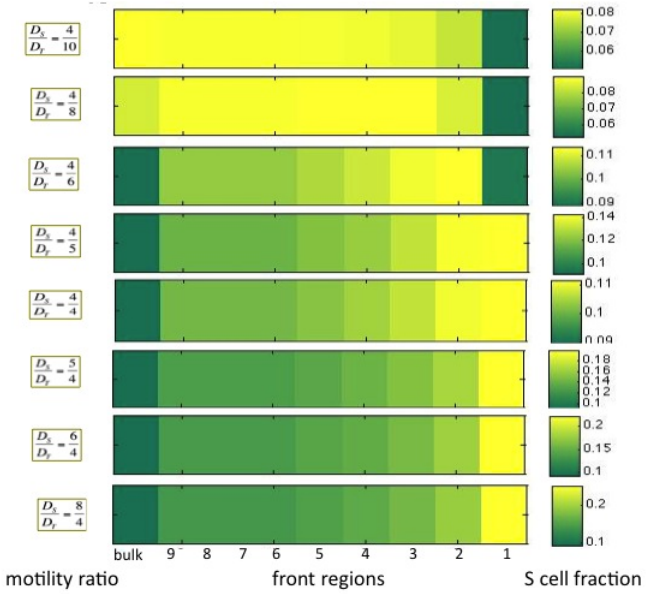

(b) S cell fraction as a function of front regions

Figure 5: **The effect of different motilities on front speed:** In a) front position is shown as a function of different ratio of cell motilities (D_S/D_T) at a fixed time T=15000. Each data point is an average over 30 simulations. Front position is defined to be the overall mean of the cell positions in the front region. b) S cell fraction is shown in different regions of the 9 quantiles of the front and the bulk. In general as the ratio of S over T cell motility decreases results in less S cell fraction in the more advanced front quantiles as well as S cell fraction in bulk which creates a slower front. This pattern does not follow for the case $D_S/D_T = 1$ since as we see in this case the tip S cell density (regions 1, 2, 3) is at 0.11, where for $\frac{5}{4}$ is 0.18 and $\frac{4}{5}$ is 0.14.

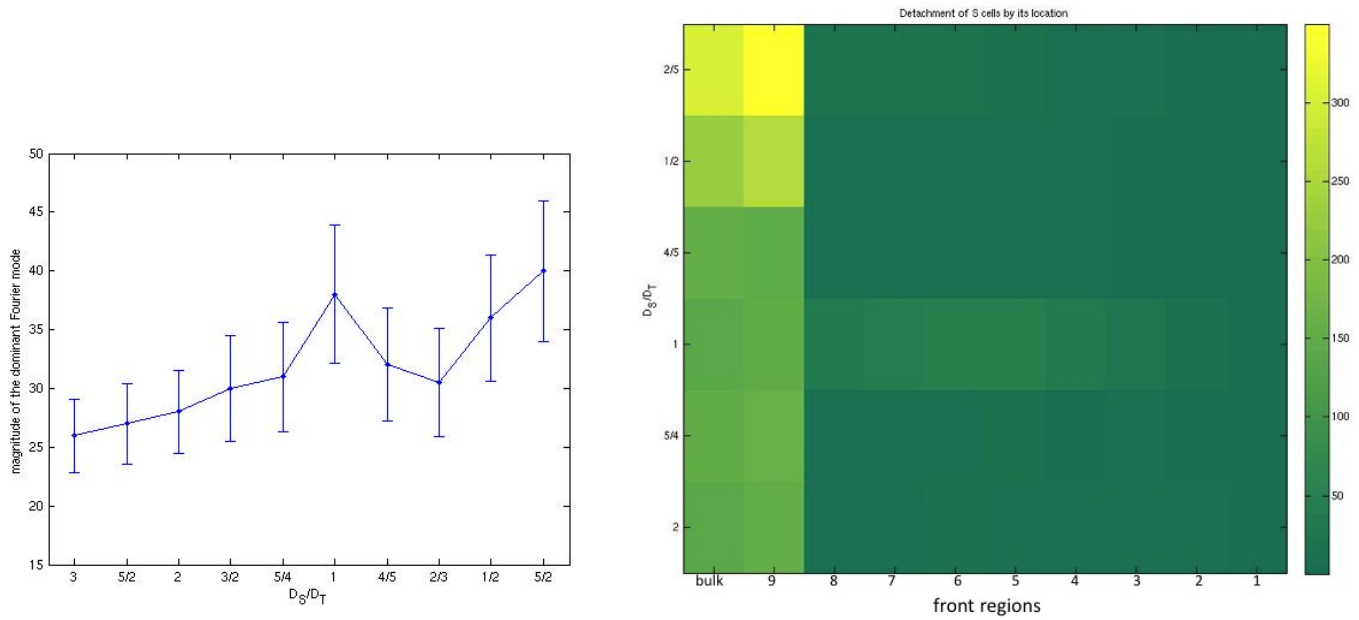

(a) dominant mode magnitude

(b) S cell detachment as a function of front regions

Figure 6: **The effect of different motilities on front instability:** In a) magnitude of the Fourier dominant mode is shown as a function of different ratio of cell motilities (D_S/D_T) at a fixed time T=15000. Each data point is an average over 30 simulations and bars show standard deviation at each point. b) Detachment of S cell fraction is shown in different regions of the 9 quantiles of the front and the bulk. As the ratio S over T cell motility decreases results in more S cell detachment specifically in the lower front regions. This creates larger instability. When $D_S/D_T = 1$, we see a pick in the instability diagram which can be explained by looking at the regions of S cell detachment in the front. In this case we see larger detachment of S cell from all the quantiles of the front which is different from other motility ratio cases. We quantify the detachment of S cells by calculating maximum distance of a S cell from other cells over all rows at the time step.

Tables

Table 1: **Summary of parameters effect on front invasiveness**

observation/ parameters ↑	front speed	instability
N (node capacity)	decreasing	decreasing
α (feedback strength)	decreasing	increasing

↑ means parameters in the table are increasing

Table 2: **Summary of different cell type motilities effect on front invasiveness**

observation/ motilities	front speed	instability
$D_S = D_T$	control	control
$D_S > D_T$	high	low
$D_S < D_T$	low	constant

Same motility case is a control and two other motility types are compared with the control.

References

[1] Lander, A.D., Gokoffski, K. K., Wan, F. Y. M. , Nie, Q. & Calof, A. L. 2009 *Cell lineages and the logic of proliferative control.* PLoS Biol 7(1): e1000015. doi:10.1371/journal.pbio.1000015

[2] Lo, W. C., Chou, C., Gokoffski, K. Wan, F. Y. M., Lander, A. D., Calof, A. L. & Nie, Q. 2009 *Feedback regulation in multistage cell lineages.* Mathematical Biosciences and Engineering, vol. 6, pp. 5982

[3] N. Boccara *Modeling Complex Systems* Springer 2004

[4] D. Rothman, S. Zaleski *Lattice Gas Cellular Automata, Simple models of Complex Hydrodynamics.* Cambridge University Press, ISBN 0-521-55201 1997.

[5] J. Hardy and Y. Pomeau und O. de Pazzis *Time Evolution of a Two-Dimensional Classical Lattice System.* Phys. Rev. Lett., vol. 31, pages 276 279, 1973. 11

[6] H. Hatzikirou, L.Brusch, A. Deutsch *From Cellular Automata rules to a macroscopic mean-field description* . Acta Physica Polonica B Proceedings Supplement, Vol 3 2010.

[7] Hatzikirou, H., Basanta, D., Simon, M., Schaller, K. & Deutsch, A. 2010 *Go or Grow: the key to the emergence of invasion in tumor progression?* . Mathematical Medicine and Biology, doi:10.1093/imammb/dqq011

[8] Sottoriva, A., Sloot, P. M. A., Medema, J. P. & Vermeulen, L. 2010 *Exploring cancer stem cell niche directed tumor growth.* Cell Cycle, vol. 9 (8), pp 1472-1477

[9] Sottoriva, A., Verhoeff, J. C., Borovski, T., McWeeney, S. K., Naumov, L., Medema, J. P., Sloot, P. M. A. & Vermeulen, L. 2010 *Cancer Stem Cell Tumor Model reveals invasive morphology and increased phenotypical heterogeneity* Cancer Res, vol. 70, pp 46-56

[10] Enderling, H., Hlatky, L. & Hahnfeldt, P. 2009 *Migration rules: tumors are conglomerates of self-metastases*, British Journal of Cancer, vol. 100 (12), pp. 1917-25.

[11] Enderling, H., Park, D., Hlatky, L. & Hahnfeldt, P. 2009 *The importance of spatial distribution of stemness and proliferation state in determining tumor radio response.* Math. Model. Nat. Phenom., vol. 4(3), pp. 117-133.

[12] Enderling, H., Hlatky, L. & Hahnfeldt, P. 2010 *Tumor morphological evolution: directed migration and gain and loss of the self-metastatic phenotype.* Biology Direct 5-23, http://www.biology-direct.com/content/5/1/23

[13] A. Deutsch, S. Dormann *Cellular Automaton Modeling of Biological Pattern Formation Characterization, Applications and Analysis.* Birkhauser, ISBN 0-8176-4281-12005.

[14] M. Boerlijst, Math. Biosc. 200, 118 (2006).

[15] M. Al-Hajj, M.S. Wicha, A. Benito-Hernandez, S.J. Morrison, M.F. Clarke. *Prospective identification of tumorigenic breast cancer cells.* Proc Natl Acad Sci USA (2003) vol. 100 (7) pp. 3983-8.

[16] J.E. Visvader, G.J. Lindeman. *Cancer stem cells in solid tumors: accumulating evidence and unresolved questions.* Nat Rev Cancer (2008) vol. 8 (10) pp. 755-68.

[17] E. Charafe-Jauffret, C. Ginestier, D. Birnbaum. *Breast cancer stem cells: tools and models to rely on.* BMC Cancer (2009) vol. 9 pp. 202.

[18] D.D. Hemmati, I. Nakano, J.A. Lazareff, M. Masterman-Smith, D.H. Geschwind, M. Bronner-Fraser, H.I. Kornblum. *Cancerous stem cells can arise from pediatric brain tumors.* Proc Natl Acad Sci USA (2003) vol. 100 (25) pp. 15178-83.

[19] S.K. Singh, C. Hawkins, I.D. Clarke, J.A. Squire, J. Bayani, T. Hide, R.M. Henkelman, M.D. Cusimano, P.B. Dirks. *Identification of human brain tumor initiating cells.* Nature (2004) vol. 432 (7015) pp. 396-401.

[20] A.T. Collins. *Prospective Identification of Tumorigenic Prostate Cancer Stem Cells.* Cancer Research (2005) vol. 65 (23) pp. 10946-10951.

[21] D. Fang. *A Tumorigenic Subpopulation with Stem Cell Properties in Melanomas.* Cancer Research (2005) vol. 65 (20) pp. 9328-9337.

[22] E. Monzani. F. Fachetti, E. Galmozzi, E. Corsisni, A. Benetti, C. Cavazzin, A. Gritti, A. Piccinini, D. Porro, M. Santinami, G. Invernici, E. Parati, E. Alessandri, C.A.M. La Porta. *Melanoma contains CD133 and ABCG2 positive cells with enhanced tumorigenic potential.* Eur. J. Cancer (2007) vol 43 pp 935-946.

[23] C.A. O'Brien, A. Pollett, S. Gallinger, J.E. Dick. *A human colon cancer cell capable of initiating tumor growth in immunodeficient mice.* Nature (2007) vol. 445 (7123) pp. 106-110.

[24] L. Ricci-Vitiani, D.G. Lombardi, E. Pilozzi, M. Biffoni, M. Todaro, C. Peschle, R. De Maria. *Identification and expansion of human colon-cancer-initiating cells.* Nature (2007) vol. 445 (7123) pp. 111-115.

[25] S. Yin, J. Li, C. Hu, X. Chen, M. Yao, M. Yan, G. Jiang, C. Ge, H. Xie, D. Wan, S. Yang, S. Zheng, J. Gu . *CD133 positive hepatocellular carcinoma cells possess high capacity for tumorigenicity* . Int. J. Cancer (2007) vol 120 pp 144-1450.

[26] S. Ma, K.-W.W. Chan, L. Hu, T.K. Lee, J.Y. Wo, I.O. Ng, B.-J.J. Zheng, X.-Y.Y. Guan. *Identification and characterization of tumorigenic liver cancer stem/progenitor cells.* Gastroenterology (2007) vol. 132 (7) pp. 2542-56.

[27] M.M. Ho, A.V. Ng, S. Lam, J.Y. Hung. *Side Population in Human Lung Cancer Cell Lines and Tumors Is Enriched with Stem-like Cancer Cells.* Cancer Research (2007) vol. 67 (10) pp. 4827-4833.

[28] M. S. Wicha, S. Liu, G. Dontu *Cancer Stem Cells: An Old Idea-A Paradigm Shift.* American Association for Cancer Research 2006

[29] T. Lapidot, C. Sirard, J. Vormoor, B. Murdoch, T. Hoang, J. Caceres-Cortes, M. Minden, B. Paterson, M.A. Caligiuri, J.E. Dick. *A cell initiating human acute myeloid leukemia after transplantation into SCID mice.* Nature (1994) vol. 367 (6464) pp. 645-8.

[30] D. Bonnet, J.E. Dick. *Human acute myeloid leukemia is organized as a hierarchy that originates from a primitive hematopoietic cell.* Nat Med (1997) vol. 3 (7) pp. 730-7.

[31] V. Cristini, J. Lowengrub, Q. Nie Nonlinear simulation of tumor growth J. Math. Biol. 46, 191224 2003

[32] J S Lowengrub, H B Frieboes, F Jin, Y-L Chuang, X Li, P Macklin, S M Wise, V Cristini *Nonlinear modeling of cancer: bridging the gap between cells and tumors.* Iposcience (2010) No. 23

[33] T. Watabe, K. Miyazono. *Roles of TGFβ family signaling in stem cell renewal and differentiation.* Cell Res (2009) vol. 19 (1) pp. 103-15.

[34] J. Anido, A. Sez-Borderas, A. Gonzlez-Junc, L. Rodn, G. Folch, M.A. Carmona, R.M Prieto-Snchez, I. Barba, E. Martnez-Sez, L. Prudkin, I. Cuartas, C. Ravents, F. Martnez- Ricarte, M.A. Poca, D. Garca-Dorado, M.M. Lahn, J.M. Yingling, J. Rodn, J. Sahuquillo, J. Baselga, J. Seoane. *TGFβ Receptor Inhibitors Target the CD44(high)/Id1(high) Glioma-Initiating Cell Population in Human Glioblastoma.* Cancer Cell (2010) vol. 18 (6) pp. 655-68.

[35] E. Meulmeester, P. Ten Dijke. *The dynamic roles of TGF-β in cancer.* J Pathol (2011) vol. 223 (2) pp. 205-18.

[36] Hanahan and R. Weinberg *The hallmarks of cancer Cell* Vol. 100, pages 57-70, 2000.

[37] P. C. Nowell. *The clonal evolution of tumor cell populations.* Science (1p76) vol. 194, pages 2328, 1976

[38] Furth et al., J. Furth, G. Ueda and K.H. Clifton In: H. Busch, Editor, Methods in Cancer Research Vol. 10, Academic Press, New York (1973), pp. 201277 Ch 8.

[39] W.S. Bullough. *Mitotic and functional homeostasis: a speculative review.* Cancer Research (1965) vol. 25 (10) pp. 1683-727.

[40] A.C. McPherron, A.M. Lawler, S.L. Lee. *Regulation of skeletal muscle mass in mice by a new TGFβ superfamily member.* Nature (1997) vol. 387 (6628) pp. 83-90.

[41] D. Hanahan, R. A. Weinberg *Hallmarks of Cancer: The Next Generation* Cell (2011), DOI 10.1016/j.cell.2011.02.013

[42] C.-S. Chou, W.-C. Lo, K.K. Gokoffski, Y.-T. Zhang, F.W. Wan, A.D. Lander, A.L. Calof, Q. Nie. *Spatial Dynamics of Multistage Cell Lineages in Tissue Stratification.* Biophysj (2010) vol. 99 (10) pp. 3145-3154.

[43] Drasdo D. *On selected individual-based approaches to the dynamics of multicellular systems.* In: Alt W, et al., editors. Multiscale Modeling. Birkhauser; Basel: 2003.

[44] Hatzikirou H, Deutsch A, Schaller C, Simon M, Swanson K. *Mathematical modeling of glioblastoma tumor development: A review.* Math. Models Methods Appl. Sci. 2005;15:177994.

[45] Zhang L, Wang Z, Sagotsky JA, Deisboeck TS. *Multiscale agent-based cancer modeling.* J Math Biol. 2009

[46] Quaranta V, Rejniak K, Gerlee P, Anderson ARA. *Invasion emerges from cancer cell adaptation to competitive micro-environments: quantitative predictions from multiscale mathematical models.* Sem. Cancer Biol. 2008;18:33848.

[47] Bearer EL, Lowengrub JS, Chuang YL, Frieboes HB, Jin F, Wise SM, Ferrari M, Agus DB, Cristini V. *Multi-parameter computational modeling of tumor invasion.* Cancer Res 2009;69:4493501. [PubMed: 19366801]

[48] Youssefpour, H., Li, X., Lander, A. D. & Lowengrub, J.S. 2011 *Multispecies model of cell lineages and feedback control in solid tumors* Under print 2011

[49] S.M. Ross, *Introduction to Probability Models* eight edition, Academic Press, An imprint of Elsevier

[50] B. Chopard and M. Droz. *Cellular automata modeling of physical systems.* Cambridge University Press, Cambridge, 1998. 25, 31, 32, 49

[51] Zhong- Ying Chen *Noise-induced instability* PHYSICAL REVIEW 1990, A VOLUME 42, NUMBER 10

[52] Y. Ito *Social Behaviour of a Subtropical Paper Wasp, Ropalidia fasciata (F.) Field Observations during Founding Stage* J. of Ethology 1983.

[53] H. W. Kang, L. Zheng, H. G. Othmer *A new method for choosing the computational cell in stochastic reactiondiffusion systems* J. Math. Bio. 2011

[54] L. Billings and I. B. Schwartz *Exciting chaos with noise: unexpected dynamics in epidemic outbreaks* J. Math. Bio. 2007